Local Burning Rates and Heat Flux for Boundary Layer Diffusion Flames Under Forced Flow

Ajay V. Singh[a] and Michael J. Gollner[b]
University of Maryland, College Park, MD, 20742

A methodology based on the Reynolds analogy was developed earlier that allowed for the estimation of local mass burning rates and heat fluxes in free-convection laminar boundary-layer diffusion flames. In this study, the relationship was examined in a forced-convective environment using methanol as a liquid fuel. The gas phase temperature profiles across the laminar boundary layer with a methanol diffusion flame established over it were measured with the free-stream air flowing parallel to the condensed fuel surface. Local and averaged mass burning rates were measured along with shear stresses at the fuel surface. The fuel consumption rate and flame lengths were observed to increase monotonically with an increase in the free-stream velocity. While the initial study was taken in the laminar regime, further extensions of the technique could be applicable to turbulent boundary layer combustion in propulsion-oriented research.

[a] Graduate Student, Department of Fire Protection Eng., University of Maryland College Park, AIAA Member.
[b] Assistant Professor, Department of Fire Protection Eng., University of Maryland College Park, AIAA Member.

Nomenclature

B = B-number (Spalding mass transfer number) (-)

C_f = Local friction coefficient (-)

c_p = Specific heat at constant pressure (J/kg-K)

D = Species diffusivity (m^2/s)

d = Diameter (m)

h = Convective heat transfer coefficient (W/m^2-K)

k = Thermal conductivity (W/m-K)

L = Length of the condensed fuel surface (m)

L_v = Effective heat of vaporization (J/kg)

$\dot{m}_f^{''}$ = Mass-burning rate (mass flux) (kg/m^2-s)

Nu = Nusselt number (-)

Pr = Prandtl number (-)

$\dot{q}_{fl,c}^{''}$ = Flame convective heat flux (W/m^2)

$\dot{q}_{fl,r}^{''}$ = Flame radiative heat flux (W/m^2)

$\dot{q}_{net}^{''}$ = Net heat flux (W/m^2)

$\dot{q}_{s,rr}^{''}$ = Surface re-radiation heat flux (W/m^2)

$\dot{q}_{s,i}^{''}$ = Surface incident heat flux (W/m^2)

t = Time (s)

T = Temperature (K)

U_∞ = Free-stream velocity (m/s)

x = Coordinate parallel to the condensed fuel surface (m)

x^* = Non-dimensional distance, x/L (-)

X_f = Flame length (m)

y = Coordinate perpendicular to the condensed fuel surface (m)

y^* = Non-dimensional distance, y/L (-)

y_f = Flame standoff distance (m)

Greek Symbols

α = Thermal diffusivity (m^2/s)

ε = Emissivity (-)

ν = Kinematic viscosity (m^2/s)

ρ = Density (kg/m^3)

σ = Stefan-Boltzmann constant (5.67×10^{-8} $W/m^2\text{-}K^4$)

τ_s = Shear stress at the fuel surface (N/m^2)

Subscripts

ad = Adiabatic

tc, b = Thermocouple junction or bead

f = Film (mean properties)

fl = Flame

g = Gas

∞ = Ambient

p = Pyrolysis

s = Surface

w = Wall/Wire

Abbreviations

HFG = Heat flux gauge

LBL = Laminar boundary layer

PMMA = Poly methyl methacrylate

I. Introduction

Boundary layer combustion has been previously investigated in connection with various applications such as ablative cooling, erosive burning of solid propellants and surface combustion of liquid fuels. While there are several studies [1–11] in the literature that have investigated boundary layer combustion, experimental investigations are limited despite its practical importance. In order to gain more fundamental knowledge of boundary layer combustion processes, it is necessary to

estimate both local burning rates and incident flame heat fluxes to the condensed fuel surface, as these coupled processes control flame stabilization and thrust for applications such as hybrid rocket propulsion.

The rate of combustion of fuel depends upon mass and heat transfer processes. In a jet or fuel surface combustion, the rate of combustion depends upon the heat and mass transfer processes responsible for heating and evaporating the liquid fuel and diffusing it to meet the oxygen required for combustion [1]. Heat transfer from the reaction zone to the unburnt material has been considered to take place mainly through the gas phase. The amount of heat transferred from the gas phase to the condensed phase depends on the temperature profile in the gas phase adjacent to the combustible surface, and is closely related to the behavior of gasified fuel, air and combustion products.

A methodology based on the Reynolds analogy was developed earlier [10, 11] that allowed for the estimation of local mass burning rates effectively in free-convective laminar boundary-layer diffusion flames. By extension of the Reynolds Analogy, it was hypothesized that the non-dimensional temperature gradient at the surface of a condensed fuel is related to the local mass burning rate through some constant of proportionality. This proportionality was tested and verified by conducting experiments in a free-convective environment using methanol and ethanol as liquid fuels and PMMA as a solid fuel where fine-wire thermocouples were used to get detailed temperature profiles in the vicinity of combustible surfaces [10, 11]. The method has its basis in the Chilton-Colburn [12] extension to the Reynolds analogy [13] that establishes a relationship between mass, momentum, and heat transfer in a boundary layer over a solid or liquid fuel surface,

$$\frac{\tau_s}{U_\infty \nu^{2/3}} \equiv \frac{h}{c_p \alpha^{2/3}} \equiv \frac{\dot{m}''}{D^{2/3} ln(1+B)}. \tag{1}$$

Emmons hypothesized that the shear stress at the surface of a combusting fuel must be proportional to the mass burning rate [1]. Using Eqn. (1), Emmon's hypothesis (outlined in Eq. 5) and a heat transfer coefficient at the surface of a flat fuel [11], an expression for the local mass burning rate can be derived. By extension of the Reynolds Analogy, it was hypothesized that the non-dimensional temperature gradient at the surface of a condensed fuel is related to the local mass burning rate through some constant of proportionality [11] and is given by

$$\dot{m}''_f = \frac{C}{L}\left(\frac{\partial T^*}{\partial y^*}\right)_{y^*=0} = \frac{Bk_w}{c_p L}\left(\frac{\partial T^*}{\partial y^*}\right)_{y^*=0}, \tag{2}$$

where $T^* = (T - T_{w,p}/T_{fl,ad} - T_{w,p})$ represents the non dimensional temperature, $T_{w,p}$ and $T_{fl,ad}$ represent the wall (taken as the pyrolysis temperature of the given fuel) and adiabatic flame temperature, respectively for a given fuel, L is a length scale representing the length of the region that is pyrolyzing or vaporizing and $y^* = (y/L)$ denotes the non-dimensional normal direction with reference to the surface that is issuing fuel vapor. The definition of the non-dimensional temperature was chosen so that the boundary layer equations can be properly normalized. Also, defining T^* in the manner outlined above helps in making the relationship universally applicable over a wide range of fuels and geometry. The proportionality constant C appearing in Eqn. (2) equals (Bk_w/c_p), where k_w is the thermal conductivity of the gas phase evaluated at the wall temperature and c_p is the specific heat measured at the adiabatic flame temperature of the given fuel. The term B that appears in Eq. (1,2) is a non-dimensional proportionality constant that relates the rate of mass transfer (e.g., vaporization, combustion) to the rate of heat transfer, and is essentially the driving force for mass transfer, and was first referred to as the “transfer number" by Spalding [14]. The Prandtl number, Pr, is assumed to be equal to unity.

The aim of the present study is to use the above relationship (defined in Eqn. 2) for estimation of local mass burning rates and flame heat fluxes. Temperature profiles across the boundary layer with a diffusion flame established over a liquid fuel (methanol) with a free stream of air parallel to the combustible surface was measured by using fine-wire thermocouples at four different free-stream velocities namely U_∞=0.79, 0.99, 1.54 and 2.06 m/s respectively. Time averaged fuel consumption rates were also measured by using a load cell. The relationship described above has been further utilized to separate the convective and radiative components of flame heat flux by carrying out an energy balance at the surface of the liquid fuel. The aim of the present study is to improve the accuracy and predictive capability of numerical models by providing an experimental data set for local burning rates and various components of incident flame heat flux to the condensed fuel surface. While the initial study was carried out in the laminar regime, further extensions of the technique could be applicable to turbulent boundary layer combustion.

II. Literature Review

The physical nature of steady, laminar diffusion flames sustained on condensed fuel surfaces have been investigated by a number of researchers in the past. Burke and Schumann [15] were one of the earliest researchers to present a theoretical analysis of a general diffusion flame from homogeneous reactants. They solved the problem of flame zone in concentric duct burners with a gaseous fuel flowing in the core and air flowing in the annular regions. Spalding [16] addressed the problem of fuel pyrolysis due to energy transfer from combustion zone. The modern era of studies on diffusion flame with application to fire safety, began with the pioneering work on mathematical modeling of steady flame carried out by Emmons [1]. A similarity solution of the classical reacting boundary layer problem under a zero-gravity environment was reported. An analytical expression for the burning rate of a diffusion flame established over a horizontal liquid fuel surface that was subjected to forced air flow parallel to its surface was proposed. Emmons, in his analysis, established the foundations for the theoretical modeling of this problem. Using the boundary layer and flame sheet approximations he obtained explicit formulas for the mass burning rate in terms of the gas flow parameters and fuel properties. Due to the simplicity of the closed-form equation, Emmons classical solution was used widely and provided a starting point for flame propagation studies carried out subsequently by Kosdon et al. [2], Kim et al. [3], Pagni and Shih [6] and Annamalai and Sibulkin [8]. Kosdon et. al. and Kim et. al., applied the same methodology to develop analyses of the laminar, free convective burning of a vertical fuel surface, and conducted experiments that verified the mass burning rate predictions of the model. Much later, Pagni [17] presented a review of various aspects of classical diffusion flames relevant to fire safety. He explored, among others, problems involving forced, free, mixed, and stagnation point combusting boundary layers. Several research studies reported the use of boundary layer assumptions to describe fire related parameters such as the flame length [6], flame spread rate [8], and flame standoff distance [18]. Extensive reviews on the application of the Emmons model, to predict laminar flame propagation on liquid and solid fuel surfaces, are also found in the works of Sirignano [19] and Williams [20].

Experimental studies followed analytical work, investigating various aspects of non-spreading, steady, boundary layer type diffusion flames. One of the earliest experimental investigations on the

aerodynamic structure and stability of diffusion flames stabilized over a fuel surface was reported by Hirano and co-authors [4, 5], where gaseous fuels were injected uniformly through a porous flat plate into a parallel air stream. These experiments showed that the aerodynamic structure of the boundary layer is significantly different in the presence of a diffusion flame when compared to the boundary layer without a flame. Both velocity as well as temperature profiles were obtained at various locations along the plate surface. In their subsequent experimental studies, Hirano and Kinoshita [21] measured gas velocities and temperature profiles across a diffusion flame established over a liquid fuel surface with a free air stream parallel to the plate. Later, Andreussi and Petarca [9] carried out experiments similar to those by Hirano and Kinoshita [21] using ethyl alcohol as a fuel. Both authors studied the structure of the diffusion flame formed on a liquid surface with a parallel oxidizer flow experimentally, analytically or both. Andreussi and co-authors [22] later developed a theoretical model based on the Shcvab-Zeldovich formulation of the problem. In a subsequent study, Andreotti and co-authors [23] completed the analysis of boundary layer diffusion flames with measurements of velocity profiles, fuel-burning rates and temperature profiles over a wide range of conditions for various liquid fuels. Gas velocity and temperature profiles were measured by Hirano and Kinoshita whereas Andreussi and co-authors measured the temperature, velocity and species concentration profiles across the boundary layer diffusion flame. However, previous studies did not measure the local temperature gradients at the surface of a condensed fuel and no attempt was made to measure the local fuel consumption rate. A recent study by Singh et. al. [10, 11] utilized a first set of temperature measurements close to the fuel surface of buoyant methanol, ethanol and PMMA wall flames to calculate the local mass burning rates, by using a new technique based on Eqn. (2).

III. Experimental Facility and Instrumentation

Figure 1 is a schematic of the experimental set-up, the key components of which include a wind tunnel, fuel wick holder, and thermocouples mounted on a set of Velmex X-Y unislides. The wind tunnel has a 100 $\times$ 75 $\times$ 100-cm plenum at one end into which an Ebm papst (G3G250-MW72-01) variable speed blower pressurizes the air. This pressure buildup in the plenum drives the flow of the air through the wind tunnel; hence, the effects of the blower on the flow are minimized. A

30.48-cm converging section connects the plenum to the 122-cm straight section, which has a 30.48 $\times$ 30.48-cm cross-section. A set of fine screens are placed at the entrance and exit of the converging section and a combination of turbulence reduction screens and 5-cm-thick honeycomb with 0.3-cm diameter holes is inserted 110-cm upstream from the tunnel exit to straighten the flow. The flow velocity in the wind tunnel is selected by adjusting the speed of the blower with the help of a pulse-width-modulation (PWM) controller. The fuel soaked wick is positioned outside the wind tunnel, at the center of the tunnel exit. This makes it easier for the thermocouples to be moved freely in and out of the flame to measure the gas-phase temperatures.

The sample holder sits on a load cell and consists of two U-shaped aluminum brackets that were connected to an aluminum sheet (measuring 30.48 $\times$ 60.96 cm and 1.5-mm thick) and mounted vertically atop a load cell. A sheet of ceramic fiber insulation board 1.27-cm thick, with a section 2-cm from the base of the sheet cut out for holding the fuel sample, was mounted atop the aluminum sheet. A thin metal lip measuring 40.64 $\times$ 10 cm was attached just before the leading section of the condensed fuel surface to reduce the flow separation and bluff body effects of the sample holder and to prevent the transition of a laminar boundary layer due to surface roughness of the upstream insulation board. According to Ha et. al. [24], by attaching an extension plate at the leading edge of the fuel surface, the separation of flow may be prevented and an ordinary boundary layer diffusion flame can be established. In the flow without an extension plate, the interaction between the flow separation and the diffusion flame was found to exist [24]. Therefore, our condensed fuel surface starts 10-cm away from the exit of the wind tunnel. At the measurement location, the holder is positioned with its leading edge against the wind tunnel exit at the center of the channel. As the metal sheet lip is wider (40.64-cm) than the the width of the tunnel (30.48-cm), the exiting air jet is divided into two and the top half forms a boundary layer over the sample. The front surface of the insulation wall was coated with a black radiation absorbing paint having an absorbptivity of approximately 98%. The liquid fuel wick was a 10 cm $\times$ 10-cm $\times$ 1.27 cm thick sheet of porous noncombustible material (Alkaline earth silicate wool). In order to eliminate leakage of the liquid fuel from the sides, sodium silicate was applied to all interfaces of the wick except the top face. Burning was limited to the front surface of the wick by shielding the remaining sides with aluminum

foil. During testing, the wick was soaked with liquid fuel up to its point of saturation so that it gave a stable boundary-layer diffusion flame for the longest time duration possible (enough to take precise temperature measurements). The fuel wick was soaked with approximately 120 ml of liquid fuel for each test.

The fuel burning rate was measured by monitoring the mass loss of the burning wick over a timed interval. A Mettler Toledo precision mass balance was used, which had a maximum capacity of 32.2 kg and a resolution of 0.1 g, to measure the mass-loss rate of the condensed fuel surface. The average mass-loss rate of the condensed fuel surface was determined by measuring the slope of the linear mass-loss versus time curve during steady burning. The burning rate measurements presented are averages of six tests at a given condition. The repeatability of these measurements was within 1.2% of the mean.

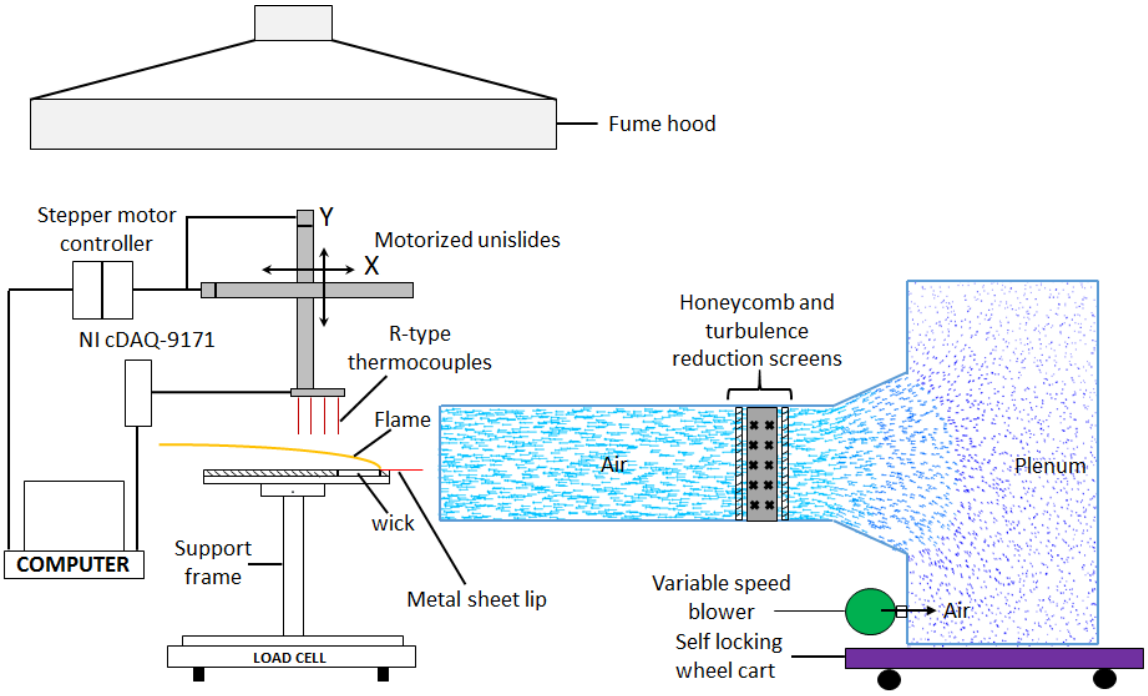

Fig. 1 Schematic diagram of the experimental setup used to measure mass-loss rates and temperature profiles over a forced-convection boundary layer diffusion flame.

Precise temperature measurements were carried out using R-type Pt/Pt-13% Rh micro thermocouples (spot welded) of 50 μm (0.002 in) and 75 μm (0.003 in) wire diameter with a bead of approximately 100 μm and 150 μm in diameter respectively (according to manufacturer's specifica-

tions). In practice, most thermocouples have bead diameters in the range 1.5 $d_w < d_b < 2.5\ d_w$ (in our case $d_b \sim 2d_w$). The micro thermocouple wires were housed in a single 1.1 mm diameter twin bore ceramic cylinder and a smaller length of thermocouple wire was exposed. Micro-thermocouples were mounted to a set of computer-controlled Velmex X-Y unislides such that they can be moved precisely up and down along the flame length or left and right across the flame thickness with a maximum spatial resolution of 1.5 μm. Voltage signals from the thermocouples were acquired, conditioned and digitized through a National Instruments NI 9214, which is a 24-bit high density 16-channel thermocouple input module which can be used up to 0.02°C measurement sensitivity. The LabVIEW software was used for synchronized motor control and continuous temperature data acquisition. Both 50 μm and 75 μm wire-diameter thermocouples were used over the same sample in order to ensure accurate radiation corrections by reading the difference between these two at the same location and applying the correlation of Collis and Williams [10, 25]. For the 50 μm wire-diameter thermocouple, a typical radiation correction at 1700 K was found to be approximately +79 K. Since the thermocouples cross regions of high temperature gradients, the measurements are expected to include conduction errors, however they have been estimated to be small here ($< 1\%$) since the heat-transfer area (the cross section of the thermocouple) is very small, therefore no corrections were made in the data for conduction errors.

Measurements of the flame stand-off distances were recorded by digital photographs, where the distance from the condensed-fuel surface to the center of the blue flame zone was measured and taken as the position of the flame. The flames were photographed in a darkened room with a side-view digital camera (Canon EOS). Before a sample was ignited, the camera was calibrated by taking a picture of a sheet of graph paper that was aligned along the horizontal axis of the fuel surface. The field of view was chosen to reduce errors in the stand-off distance measurement to less than 4%. The digital images were averaged in Matlab and flame stand-off distances were measured by using ImageJ software. In a particular test, 200 images were averaged during the steady burning regime time to obtain an averaged image. Flame stand-off measurements were carried out independently for 3 repeated tests at a given flow condition. The results were then averaged to give an averaged flame stand-off distance profile. The repeatability of these measurements was within 2% of the

mean.

Generally, in forced-flow boundary-layer flame experiments, the fuel sample is placed inside a wind tunnel. In this work, we placed the condensed fuel surface at the exit of the wind tunnel in the center of the air stream. This arrangement enabled us to obtain easy access to the boundary layer flame and condensed fuel surface for temperature and flow characterization. The wind tunnel was fully characterized for different blower speeds and velocity profiles and turbulence intensity levels were measured at the wind tunnel outlet using a Dantec Dynamics hot wire anemometer. The free-stream velocity, U_∞, was then calculated by integrating the obtained velocity profile at the tunnel outlet. The velocity data at each point was acquired with a sampling rate of 50,000 samples/s for a total duration of 10 s. The repeatability of these measurements was within 3% of the mean. The velocity profile across the tunnel outlet was found to be relatively uniform near the center. Figure 2 (a) shows the velocity profiles obtained at the wind tunnel outlet for 4 different blower speeds. To ensure that the flow is well defined at the location of the flame, we chose the dimensions of the sample to be small such that the condensed fuel surface would be within the potential flow core of the exit jet. It has been shown that velocity profiles in both X and Y directions do not change significantly within the potential core of the jet [26, 27]. Experimental measurements from Sforza and co-authors [28] show that for an air jet at the exit of a square channel, with Reynolds number Re_d between 2.6 and 8.8 $\times$ 10^4, the potential flow core length is about 5 d downstream of the exit, where d is the height of the channel. In the current work, d = 30.48 cm and hence our sample is within 1 d (20 cm from the tunnel exit). Our Re_d is between 1.5 $\times$ 10^4 and 3.9 $\times$ 10^4; therefore, the flame would be within the potential flow core of the jet. To further confirm that the velocity profiles would not change significantly within the space where the flame would exist, the velocity profiles were measured above the non-burning sample. Figure 2 (b) shows the variation of inlet velocity within the potential core of the exit jet with the streamwise distance X from the leading edge of the sample holder surface. Figure 2 (b) shows results for heights of 32, 35 and 40-mm above the sample surface at three distinct streamwise locations. The thermal boundary layer thickness at the trailing edge of the sample is approximately 30 mm for U_∞=0.79 m/s. Figure 2 (b) shows that the velocity profiles have not changed significantly within the core space where the flame is located.

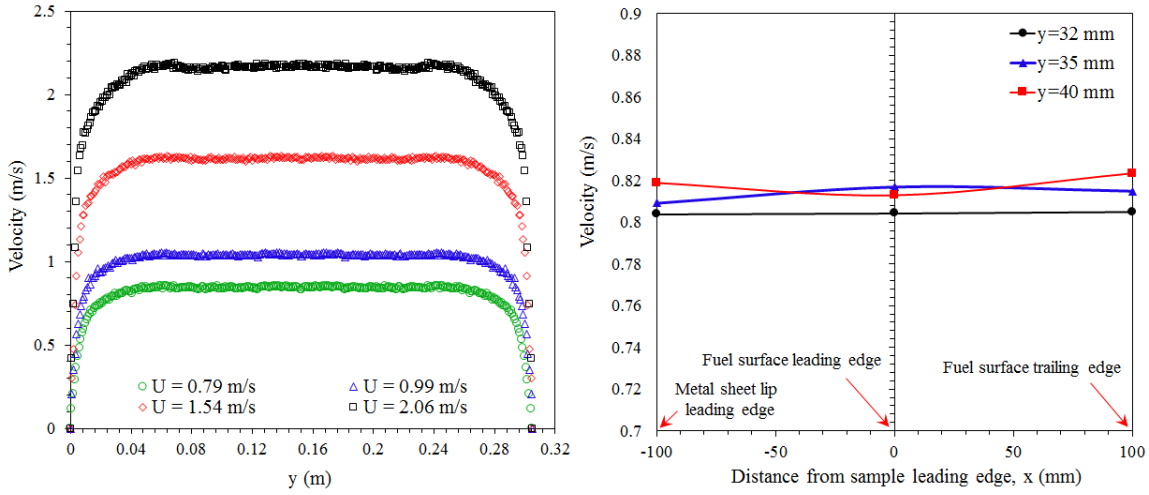

Fig. 2 (a) (left) Velocity profiles at wind tunnel outlet for different blower speeds giving an average free-stream velocity of U_∞=0.79, 0.99, 1.54 and 2.06 m/s (b) (right) Streamwise variation of air velocity beyond the tunnel exit.

A. Uncertainity Analysis

During the experimental tests, the data acquisition system acquired temperatures at 500 samples per second, providing 500 samples to average per spatial point. Reported temperatures are averages of at least five tests in a given condition and the maximum standard deviation was $< 3.2\%$ of the mean. The inherent uncertainty in temperatures measured by the thermocouple (T_{tc}) are taken to be 0.25% of the measured value based on manufacturer's specifications. The accuracy of the Nusselt number correlation used to calculate the radiation loss from the thermocouple bead was reported to be within 5% [25] and the uncertainty in k due to different species is assumed to be 3%. The error in the thermocouple emissivity (ε_{tc}) used is also small,$< \pm 3\%$, except that ε_{tc} is linear with T_{tc} so any error in T_{tc} increases the uncertainty in ε_{tc}. The Platinum emissivity was calculated using Jakob's theoretical correlation, confirmed by experimental data [29, 30] which reported the Pt emissivity uncertainty $< \pm 3\%$ when using the calculation. The uncertainty in gas temperature is then calculated from a quadratic sum of the uncertainties,

$$dT_g = \left[\left(\frac{\partial T_g}{\partial T_{tc}} dT_{tc} \right)^2 + \left(\frac{\partial T_g}{\partial \varepsilon_{tc}} d\varepsilon_{tc} \right)^2 + \left(\frac{\partial T_g}{\partial k} dk \right)^2 + \left(\frac{\partial T_g}{\partial Nu} dNu \right)^2 \right]^{1/2}. \quad (3)$$

The maximum uncertainty in gas temperatures encountered in the flame zone is then found to be within ±7 K. The maximum expanded uncertainty in gas temperatures is then found to be within ±14 K with a 95% confidence interval.

IV. Results and Discussion

A. Boundary-layer Diffusion Flames under Forced Flow

For an appropriate value of uniform air stream velocity U_∞, a stable, laminar two-dimensional diffusion flame could be established over a condensed fuel surface. When U_∞ was increased above the stability limit ($U_\infty >$ 2.2 m/s), the leading flame edge became unstable and local quenching of the flame was observed at the leading edge of the fuel surface. Increasing the flow velocities further blew off the flame completely. The flame stand-off distance was found to increase with the distance x from the leading edge. As U_∞ is increased, the flame approaches the condensed fuel surface and the flame anchoring distance was found to shift downstream. The luminosity of the blue flame zone decreased as x increased. The averaged mass burning rates and flame lengths were observed to increase monotonically with an increase of U_∞. Figure 3 shows the comparison of averaged mass burning rates and flame lengths for a methanol boundary-layer diffusion flame established under different free-stream velocities. Figure 4 shows the side-view direct flame photographs of a methanol boundary layer diffusion flame at free-stream velocities of 0.79 m/s and 2.06 m/s respectively.

It is to be noted that the Emmons solution is valid in a range of Reynolds numbers where the flame anchors near the leading edge of the methanol pool or condensed fuel surface and the combustion zone is confined around the hydrodynamic and thermal boundary layers. However, in cases of very low free-stream velocities the combustion zone is beyond the boundary layer zone and the Emmons solution deviates [31]. In cases of very high free-stream velocities, the flame moves away from the leading edge and anchors at a location downstream. The Emmons solution is not applicable in this case as well [31]. In the present work, free-stream velocities were carefully chosen in the range where Emmons solution is valid.

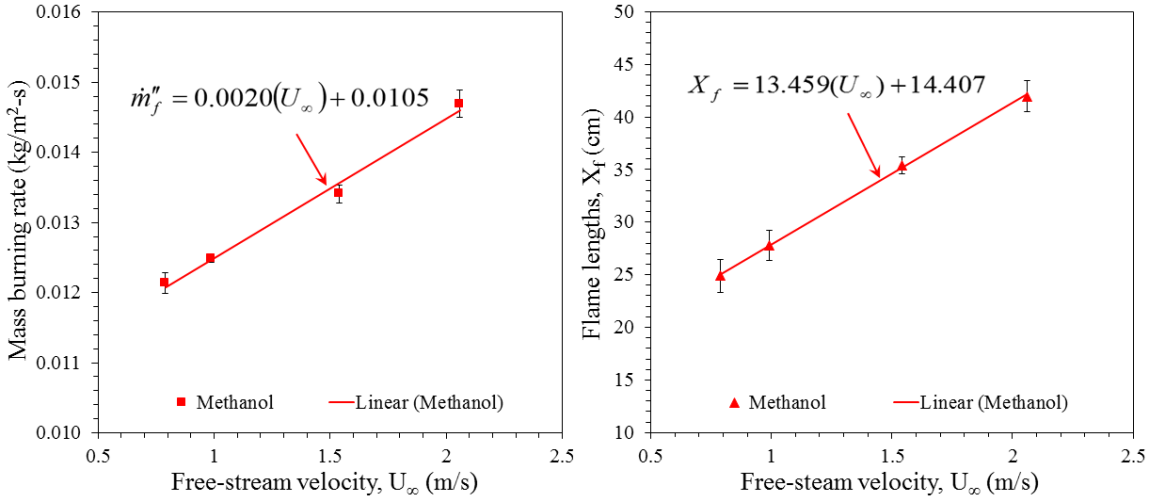

Fig. 3 Averaged mass burning rates (left) and flame lengths (right) for a methanol boundary-layer diffusion flame.

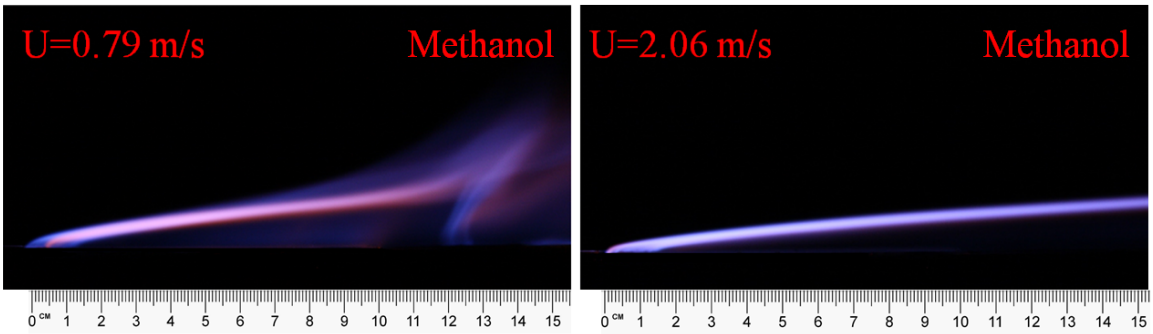

Fig. 4 Side-view photograph of a methanol boundary-layer diffusion flame at U_∞=0.79 and 2.06 m/s respectively.

B. Gas-phase Temperature Profiles

Using the experimental apparatus described above, measurements were taken for local temperature profiles along condensed fuel surfaces. Figure 5 shows the temperature profiles at several stream-wise locations along the condensed fuel surface for a methanol boundary-layer diffusion flame at free-stream velocities of 0.79 and 2.06 m/s respectively.

On the downstream side of the leading flame edge, T increases with y to a maximum flame temperature T_{fl} at the flame zone. On the air-stream side of the flame zone, T decreases with y to ambient temperature at the thermal boundary layer edge. T_{fl} at a given streamwise location was found to increase slightly with an increase in U_∞. Within about 2-3 cm of the leading edge of the

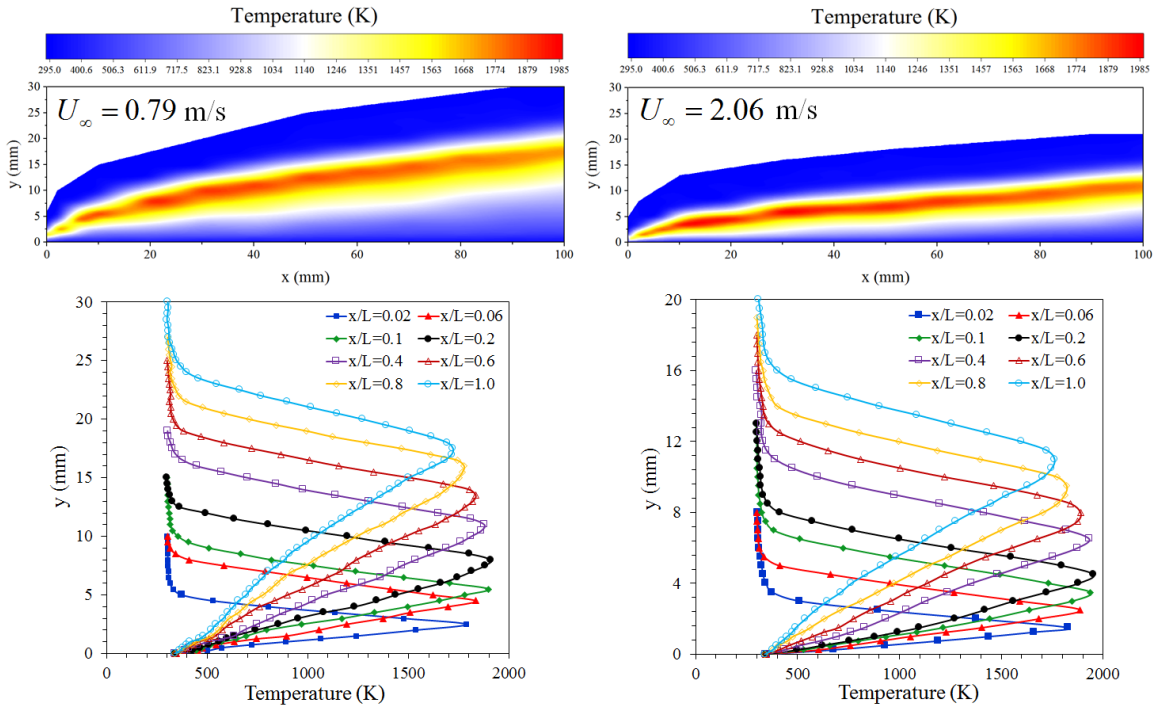

Fig. 5 (left) Gas-phase temperature contours and profiles for a methanol boundary-layer diffusion flame at $U_\infty = 0.79$ m/s (right) Gas-phase temperature contours and profiles for a methanol boundary-layer diffusion flame at $U_\infty = 2.06$ m/s.

condensed fuel surface, T_{fl} increases in the x direction. Further downstream, T_{fl} decreases in the x direction. The same observation were made by Hirano and co-authors [4] when they studied ethanol and methanol diffusion flames in a forced convective environment. The peak flame temperature was found to be 1906 K and 1980 K for U_∞=0.79 and 2.06 m/s respectively. At the trailing edge of the sample, the peak flame temperature drops by about 186 K and 219 K for free-stream velocities of 0.79 and 2.06 m/s respectively. This temperature decrease is primarily due to convective heat losses. The temperature of the condensed fuel surface was found to be approximately near the boiling point of methanol at different forced flow conditions. Observation of the temperature gradients normal to the fuel surface suggests that they are highest near the leading edge and decrease further downstream. The temperature gradient $(\partial T/\partial y)_0$ at $y = 0$ decreases in the x direction downstream of the leading edge. $(\partial T/\partial y)_0$ at a given streamwise location was found to increase with an increase in U_∞. This is consistent with known characteristics of boundary-layer diffusion flames, in that convective heat feedback decreases with x for a particular U_∞ and increases at a given streamwise location with

an increase in U_∞. The local mass-loss rate from the fuel, driven by convective heat fluxes to the surface in these small, laminar flames, should similarly decrease with x. The flame usually becomes thicker when moving downstream of the leading edge and the flame stand-off distance increases with increasing x. It follows, therefore, that the local mass burning-rate should also decrease with x, discussed later.

C. Flame Stand-off Distance and Non-dimensional Temperature Gradients

The flame stand-off distance y_f at different locations along the fuel surface are plotted in Figure 6 (a) for a methanol boundary-layer diffusion flame established under free-stream velocities of 0.79, 0.99, 1.54 and 2.06 m/s respectively. The flame stand-off distance is lower near the leading edge and it increases further downstream up to the trailing edge. This leads to enhanced heat transfer to the fuel surface at the leading edge and hence higher evaporation rates of the fuel at this location. Accordingly, the local burning rate is highest at this location. The flame stand-off distance is higher for the regions near the trailing edge and hence heat transfer at these locations is lower. Due to lower heat transfer rates at these locations, the local mass-burning rates are found to be lower at these locations. Also, the flame stand-off distance is almost proportional to $x^{0.5}$, confirming the similarity theory for a forced-convection boundary layer adjacent to a horizontal flat plate [1, 32]. As U_∞ is increased, the flame approaches the condensed fuel surface and the flame anchoring distance was found to shift downstream.

Figure 6 (b) shows the variation of the normal non-dimensional temperature gradient along the fuel surface extracted from experimental temperature data of a methanol diffusion flame for U_∞=0.79 m/s and 2.06 m/s. The normal non-dimensional temperature gradients at the fuel surface, $(\partial T^*/\partial y^*)\,|_{y^*=0}$ were calculated from the slope at $y^* = 0$ of a fifth-order polynomial fit to the non-dimensional temperature distribution near the fuel surface. The temperature gradient normal to the fuel surface was found to be highest at the leading edge and lowest at the trailing edge (x = 100 mm). The local mass-burning rate should follow a similar trend, as is revealed by the calculated rates in Figure 7.

Averaging the non-dimensional temperature gradient for the entire fuel surface, the average mass-burning rate is estimated to be 12.38 g/m^{2}s, 13.47 g/m^{2}s, 14.56 g/m^{2}s and 15.96 g/m^{2}s

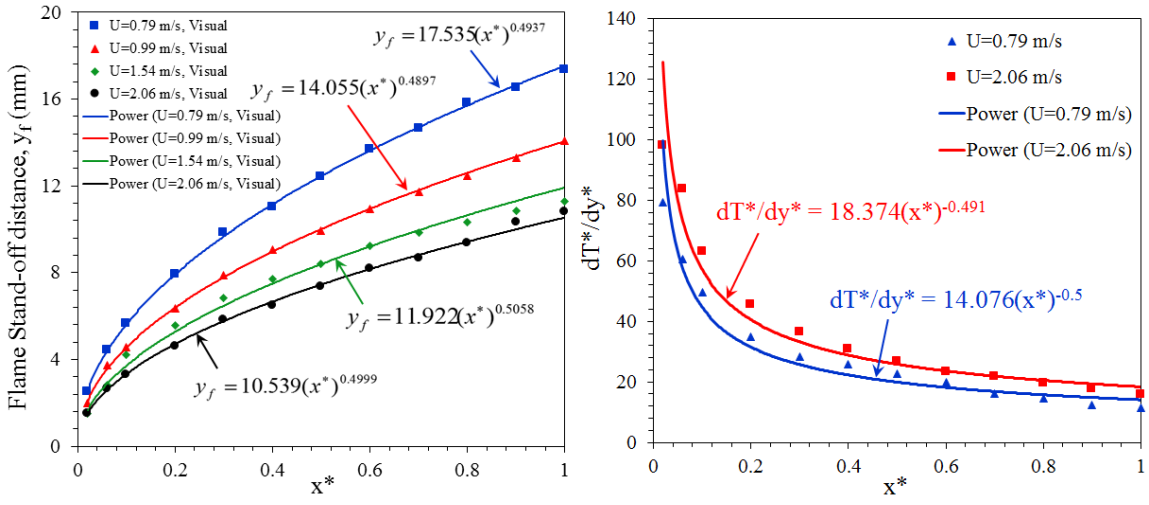

Fig. 6 (a)(left) Flame stand-off distance for a methanol boundary-layer diffusion flame established under different free-stream velocities (b)(right) Non-dimensional temperature gradients at the methanol condensed fuel surface along its length for U_∞=0.79 and 2.06 m/s.

for U_∞=0.79, 0.99, 1.54 and 2.06 m/s respectively, using Eq. (2). Appropriate average values of transport properties were used to calculate the constant C in Eq. (2) and are given in Table 1. It is to be noted that we evaluated the transport properties following the work of Kim et al. [3] where they evaluated the value of k at the wall and the value of c_p at the adiabatic flame temperature of the given fuel. The assumption of a unity Prandtl number in deriving Eqn. (2) also supports such selection of transport properties, as evaulation of the transport properties at the wall, namely μ_w and k_w, and evaluation of the specific heat at the adiabatic flame temperature of the given fuel results in a unity Prandtl number. Choosing the transport properties as outlined above works well in estimating the average mass burning rates for methanol diffusion flames established under different forced flow conditions. The average mass-burning rate evaluated though the load cell data was found to be 12.14 g/m^{2}s, 12.48 g/m^{2}s, 13.41 g/m^{2}s and 14.69 g/m^{2}s for U_∞=0.79, 0.99, 1.54 and 2.06 m/s respectively . The error in the estimation of the average mass-burning rate was therefore found to be +1.98%, +7.93%, +8.57% and +8.65% for U_∞=0.79, 0.99, 1.54 and 2.06 m/s respectively.

D. Local Mass Burning Rates and Shear Stress at Fuel surface

Figure 7 (a) also shows the variation of the local mass-burning rate for methanol diffusion flames, using the theoretical correlation from Eq. (2) and the non-dimensional temperature gradients at the

Table 1 Physical properties

Properties	Methanol
Mass transfer number, B	2.5 [33]
Thermal conductivity, k_w (W/m-K) evaluated at the pyrolyzing wall temperature	0.028 [34]
Specific heat, c_p evaluated at the adiabatic flame temperature	1394.5 [34]
$T_{w,p}$ (K)	337 [33]
$T_{fl,ad}$ (K)	2150 [34]
Length of the condensed fuel surface, L (m)	0.10

condensed fuel surface. Due to the availability of fresh oxidizer, higher convective heat feedback, higher temperature gradients and lower stand-off distances near the leading edge, the local burning rate is highest here and subsequently decreases as we move downstream towards the trailing edge. The burning rate decreases, due to the lack of fresh oxidizer, lower convective heat feedback, lower temperature gradients and higher flame stand-off distances as we move downstream. Also, the local mass-burning rate for a methanol boundary-layer diffusion flame is almost proportional to $x^{-0.5}$, confirming the power-law relationship for laminar forced-convective burning on a horizontal surface [1]. The local mass-burning rate evaluated by using Eq. (2) was also compared against the theoretical mass-burning rate given by Emmons [1]. Emmons [1] carried out an exact analysis for forced convection burning of a flat plate following the well-known Blasius solution for incompressible flow. Glassman [35] presents a functional fit to the Emmons solution as,

$$\frac{\dot{m}''_f c_p x}{k} = 0.385 \left(\frac{U_\infty x}{\nu_\infty} \right)^{1/2} Pr \frac{ln(1+B)}{B^{0.15}}, \tag{4}$$

where k represents the thermal conductivity of the gas phase, c_p the specific heat of the gas phase, Pr the Prandtl number, B the mass transfer number, U_∞ the free-stream velocity, ν_∞ the kinematic viscosity of the gas phase and x the coordinate parallel to the fuel surface. The close agreement between the theoretical and experimental local mass burning rates suggest that the proposed correlation works quite well in estimating the local mass burning rates for forced convective boundary layer diffusion flames as well.

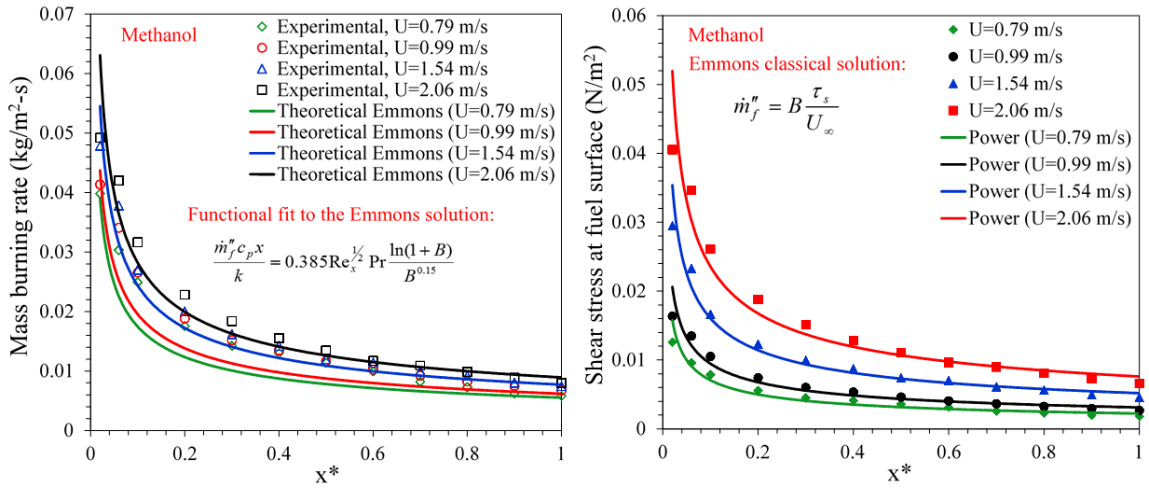

Fig. 7 (a) (left) Variation of the local mass burning rates at the condensed fuel surface along its length for U_∞=0.79, 0.99, 1.54 and 2.06 m/s.(b) (right) Distribution of shear stress at the fuel surface for a methanol boundary-layer diffusion flame at U_∞=0.79, 0.99, 1.54 and 2.06 m/s.

Emmons also hypothesized that the rate of fuel evaporation and hence the rate of burning either in the boundary layer or in the wake behind the body is related to the shear stress by

$$\dot{m}''_f = B\frac{\tau_s}{U_\infty}. \tag{5}$$

With the knowledge of local mass burning rates using Eq. (2), the shear stress at the fuel surface can be effectively calculated. Thus, the combustion rate in the boundary layer on a flat plate is simply related to the velocity gradient at the surface. Shear stress at the fuel surface follows the same power law dependence with streamwise distance x as that of the local mass burning rate and can be used to calculate the friction coefficient C_f, which can be expressed as

$$C_f = \frac{\tau_s}{\frac{1}{2}\rho_\infty U_\infty^2}. \tag{6}$$

Figure 7 (b) shows the shear stress distribution at the fuel surface for a methanol boundary layer diffusion flame for U_∞=0.79,0.99, 1.54 and 2.06 m/s respectively.

E. Wall Heat Fluxes in the Pyrolysis Zone

Utilizing gas-phase temperature measurements and local mass-burning rates, heat fluxes were evaluated in the pyrolysis zone at various stream-wise locations along the condensed fuel surface. Reasonable approximations were made to simplify the heat balance analysis. The fuel surface was assumed to be opaque with an emmissivity and aborptivity of unity. The surface radiative heat loss was given with respect to T_∞. The energy balance at the condensed fuel surface ($y = 0$) for steady burning of liquid fuels becomes

$$\dot{m}''_f L_v = \dot{q}''_{fl,c} + \dot{q}''_{fl,r} - \dot{q}''_{s,rr} \tag{7}$$

and

$$\dot{m}''_f L_v = k_w \left(\frac{dT}{dy}\right)_{y=0} + \dot{q}''_{fl,r} - \sigma\left(T_w^4 - T_\infty^4\right), \tag{8}$$

where $\dot{q}''_{fl,c}$, $\dot{q}''_{fl,r}$, $\dot{q}''_{s,rr}$ and L_v represents the convective heat flux, radiative heat flux, re-radiation heat flux from the surface and effective heat of gasification or vaporization, respectively. Here, the convective heat flux is measured by using the expression $k_w \left(\partial T/\partial y\right)_{y=0}$ which represents the gas-phase convective heating [33]. The flame imparts heat feedback to the condensed fuel surface primarily in two modes: convective and radiative. For convective-dominated steady burning, the convective heat flux from the flame is equal to $k_w \left(\partial T/\partial y\right)_{y=0}$ at the condensed fuel surface [33]. Therefore, the convective heat flux from the flame is equal to the conductive heat flux at the fuel surface for convective-dominated steady burning.

For a boundary-layer diffusion flame, the convective heat flux can be further approximated as [33],

$$\dot{q}''_{fl,c} \approx h(T_{fl} - T_w) \approx \frac{k_f(T_{fl} - T_w)}{y_f} \tag{9}$$

where

$$h \approx \frac{k_f}{y_f}. \tag{10}$$

This crude approximation allows us to calculate the convective flux in boundary-layer diffusion flames by estimating the wall (T_w) and flame temperatures (T_{fl}) at various stream-wise locations along the pyrolysis zone together with knowledge of flame stand-off distances (y_f). k_f in the above equation is the thermal conductivity of the gas phase evaluated at a mean film temperature (preferably mean of the actual flame and wall temperatures). In order to calculate convective fluxes by using Eq. (9) above, it is very important that flame and wall temperatures must be accurately determined along with precise measurements of flame stand-off distances. Errors in estimating k_f, y_f, T_{fl} and T_w could lead to serious deviations in estimating convective heat fluxes by using Eq. (9) above. However, *using temperature gradients at the fuel surface is the most accurate way to evaluate the convective heat flux* and will be compared to this crude approximation.

$\dot{q}''_{s,rr}$ can be evaluated by knowledge of the wall and ambient temperatures, respectively. Utilizing the theoretical correlation in Eqn. (2), the net heat flux, $\dot{q}''_{net}$ ($\dot{q}''_{net}$=$\dot{m}''_f L_v$), can be estimated at various stream-wise locations along the pyrolysis zone simply by the knowledge of local mass burning rates along the condensed fuel surface. The effective heat of gasification or vaporization was taken to be 1.2 kJ/g for methanol [33]. $\dot{q}''_{fl,r}$ can then easily be computed by using Eqn. (8) above. The total heat flux incident to the surface, $\dot{q}''_{s,i}$, can be defined as the sum of the convective and radiative components of the flame heat flux. Figure 8 shows the various components of flame heat flux in the pyrolysis zone of a methanol diffusion flame at U_∞=0.79 and 2.06 m/s.

Based on these results, the convective heat flux is relatively high and contributes approximately 86% of the total heat flux. The net heat feedback to the condensed fuel surface is the sum of the convective and radiative components minus reradiation from the surface. Thus, convection is the dominant mode of heat transfer and radiative contributions are small. This is reasonable for the small, laminar flames studied here. With knowledge of the local distribution of various components of heat flux, one can further compute the average value of the given components by using,

$$\dot{q}''_{avg} = \left(\frac{1}{L}\right) \int_0^L \dot{q}'' dx. \tag{11}$$

The average total incident heat flux from the flame to the wall was estimated to be 15.18 and 19.50 kW/m^2 for U_∞ = 0.79 and 2.06 m/s respectively. The average convective heat flux from

the flame to the wall was estimated to be 13.09 and 16.97 kW/m^2, for $U_\infty = 0.79$ and 2.06 m/s respectively. The average radiative heat feedback from the flame was then calculated to be 2.09 and 2.53 kW/m^2, respectively for $U_\infty = 0.79$ and 2.06 m/s. Thus, convection is the dominant mode of heat transfer in steady laminar boundary-layer diffusion flames and is primarily responsible for the pyrolysis of fuel. Also, convective and total incident heat flux to the condensed fuel surface increases as the free-stream velocity increases. This results in higher burning rates at higher free-stream velocities.

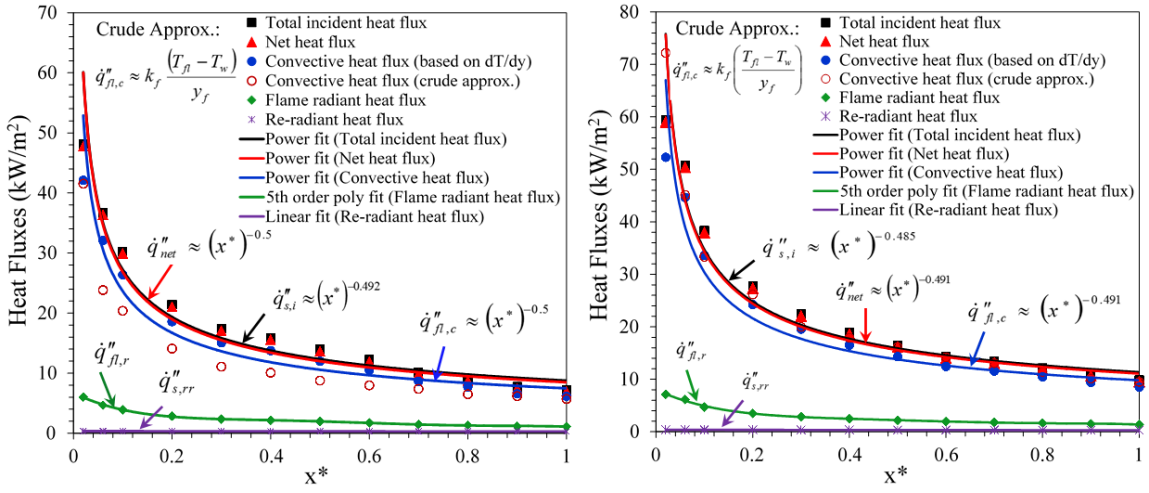

Fig. 8 Distribution of various components of flame heat flux in the pyrolysis zone for a methanol boundary-layer diffusion flame at $U_\infty = 0.79$ (left) and 2.06 m/s (right).

V. Conclusion

The gas-phase temperature profiles across a laminar boundary layer diffusion flame established over a methanol condensed fuel surface were measured for 4 different incoming flow velocities. The results suggest that local mass burning rates can be obtained from these measurements by using a theoretical correlation that is based on the Reynolds analogy. The given methodology works well for both free and forced convective boundary layer diffusion flames and is capable of giving reasonable estimates of local mass burning rates and heat fluxes in such flames. With the knowledge of local mass burning rates shear stress and hence the strain rates at the condensed fuel surface can be easily obtained. Flame stability mechanisms can thus be studied in more detail with the knowledge of these local properties. Convective heat flux was found to be the dominant mode of heat transfer

in these small laminar flames and accounted for nearly 86% of the total incident heat flux. At the condensed fuel surface, total incident heat flux was found to increase with the free-stream air velocity. This results in higher burning rates at higher free-stream air velocities. While the initial study was taken in the laminar regime, further extensions of the technique could be applicable to turbulent boundary layer combustion in propulsion-oriented research.

Appendix

Radiation Correction for the Thermocouple

The temperature measurements reported in this study have been corrected for thermocouple radiation. Flame temperature measurements across the width of the fuel sample showed no significant variation, except near the edges. Therefore, thermocouples at the center of the flame were used to produce a map of temperatures in the boundary layer by moving it across the flame (y-direction) and along the length of the flame (x-direction). Two thermocouples ($50\mu m$ and $75\mu m$ wire-diameter) were traversed along the same path at the center of the flame for accurate radiation corrections. All temperature measurements reported in this paper are an average of at least five independent tests conducted under the same conditions. In the most general case, an energy balance on the thermocouple junction takes the following form,

$$\dot{Q}_{cat} + \dot{Q}_{conv} + \dot{Q}_{rad} + \dot{Q}_{cond} = m_{tc} c_p \frac{dT_{tc}}{dt}. \tag{12}$$

with heat transfer associated with surface-induced catalytic reactions, convection between the gases and the thermocouple, radiant heat transfer between the thermocouple and its surroundings, conduction along the thermocouple wires, and transient heating or cooling of the thermocouple incorporated in Eq. (A.1). The thermocouple junction properties that characterize the transient term in the above expression include the mass of the thermocouple junction, m_{tc} and the specific heat c_p. For transient measurements, the convection and thermal inertia terms are both important, in addition to radiation. Neglecting the conduction error and errors due to catalytic effects Eq. (A.1) reduces to the following form for transient measurements,

$$(T_g - T_{tc}) = \frac{m_{tc} c_p}{h A_{tc}} \frac{dT_{tc}}{dt} + \frac{\varepsilon_{tc} \sigma}{h} \left(T_{tc}^4 - T_{surr}^4\right) \tag{13}$$

$$(T_g - T_{tc}) = \tau \frac{dT_{tc}}{dt} + \frac{\varepsilon_{tc} \sigma}{h} \left(T_{tc}^4 - T_{surr}^4\right) \tag{14}$$

where τ is the characteristic response time or time constant of the thermocouple. Eq. (A.3) shows that the time constant of the thermocouple is not only related to the physical properties of the thermocouple i.e. the mass of the thermocouple junction, m_{tc}, the specific heat, c_p, and the surface area of the junction, A_{tc}, but also depend on heat transfer coefficient of the flow, h. There is a substantial literature devoted to the measurement of time constant of the thermocouple [36–41].

For steady state measurements, as in our case, Eq.(A.1) reduces to a convective-radiative heat balance (neglecting the conduction error and errors due to catalytic effects) given by,

$$h\,(T_g - T_{tc}) = \varepsilon_{tc} \sigma \left(T_{tc}^4 - T_{surr}^4\right) \tag{15}$$

$$(T_g - T_{tc}) = \frac{\varepsilon_{tc} d_w \sigma}{k Nu} \left(T_{tc}^4 - T_{surr}^4\right). \tag{16}$$

where T_g is the real gas temperature, T_{tc} is the thermocouple junction (or bead) temperature, T_{surr} is the temperature of the surroundings, ε_{tc} is the emissivity of the thermocouple junction, σ is the Stefan-Boltzmann constant and h is the convective heat transfer coefficient of the flow over the thermocouple junction defined as $h = k\ \mathrm{Nu}/d_w$. k is the thermal conductivity of the gas, Nu is the Nusselt number, and d_w is the thermocouple wire diameter. The choice of the Nusselt number correlation is of paramount importance in calculating a radiation correction to the measured thermocouple temperature because, as shown in Eq. (A.5), the radiation correction is inversely proportional to the Nusselt number. This choice is complicated, however, due to the existence of multiple "appropriate" Nusselt number correlations and the difficulty in estimation of the properties of the gas mixture surrounding the thermocouple, particularly its thermal conductivity. The bulk

of evidence in literature, however, clearly indicates that a cylindrical Nusselt number correlation is most appropriate for describing the convective heat transfer to nearly all practical thermocouples [42], preferably that of Collis and Williams [25]. A commonly-used expression from Collis and Williams can be written as [25]

$$Nu\left(\frac{T_m}{T_g}\right)^{-0.17} = 0.24 + 0.56Re_{d_w}^{0.45} = 0.24 + 0.56\left(\frac{Ud_w}{\nu}\right)^{0.45}, \tag{17}$$

which was obtained for $0.02 < \mathrm{Re} < 44$, with the Reynolds number evaluated at the so-called film temperature, T_m the mean of the thermocouple and free-stream temperatures, i.e. $0.5\,(T_g + T_{tc})$. Here, Re is the Reynolds number defined as indicated for the local gas flow velocity, U and kinematic viscosity, ν. Substituting Eq. (A.6) into Eq. (A.5) and neglecting the small temperature dependence in Eq. (A.6), we have a system of two equations with two unknowns (namely T_g and U),

$$T_g - T_{tc_1} = \frac{\varepsilon_{tc_1} d_{w_1} \sigma}{k\left[0.24 + 0.56\left(Ud_{w_1}/\nu\right)^{0.45}\right]}\left(T_{tc_1}^4 - T_{surr}^4\right) \tag{18}$$

and

$$T_g - T_{tc_2} = \frac{\varepsilon_{tc_2} d_{w_2} \sigma}{k\left[0.24 + 0.56\left(Ud_{w_2}/\nu\right)^{0.45}\right]}\left(T_{tc_2}^4 - T_{surr}^4\right), \tag{19}$$

which demonstrates that the difference between a thermocouple reading and the actual gas temperature (i.e. the error in gas temperature measurement) increases for larger-diameter thermocouples, while it is reduced by increasing the gas flow velocity over the junction. In solving the above equations, iteration is required since the gas conductivity and kinematic viscosity are a function of the gas temperature. Initially the gas temperature is taken to be the bead temperature for the purpose of evaluating the thermal conductivity and kinematic viscosity; then, the approximate value of the gas temperature is used to re-evaluate the thermal conductivity and viscosity.

The emissivity of the bead (ε_{tc}) can also be found as a function of its temperature. In an analysis outlined by Jakob [29], Maxwell's wave equations can be solved to yield the complex indices of refraction for a metal as a function of its electrical resistivity. In the limit of low resistivity and assuming a large index of refraction, which is true for metals, Jakob [29] gives the hemispherical total emissivity of platinum (Pt) as,

$$\epsilon = 0.751\,(r_e T)^{1/2} - 0.396\,(r_e T)\,, 0 < r_e T < 0.2 \tag{20}$$

where, for platinum, r_e=$r_{e,273}T/273$, with T in K and $r_{e,273}$=11×10^{-6} Ω-cm [43]. Therefore, the platinum emissivity becomes,

$$\epsilon = 1.507 \times 10^{-4} T - 1.596 \times 10^{-8} T^2 \tag{21}$$

for $0 < T < 2230$ K. This equation is also confirmed by comparison with experimental data [30]. It was shown [30] that for temperatures where radiation is important, predicted and observed emissivities agree to within 1%. The emissivity of the thermocouple bead or junction can therefore be evaluated by using the above expression. Note that iteration is not needed for the evaluation of the platinum emissivity, since this property is a function of the junction or bead temperature, which is known.

The actual gas temperature can then be evaluated by solving Eq. (A.7) and (A.8). During experiments, the two thermocouples were traversed exactly to the same measurement points and data was sampled to account for radiation correction in the temperature measurements.

Conduction Correction for the Thermocouple

Rapid thermal conduction along thermocouple wires can result in significant heat loss from the thermocouple wire and junction to the larger, cooler lead wires or support (cooler on account of increased radiation and conductive losses through the thermocouple support structure). However, this mechanism of heat loss from the thermocouple is usually avoidable through the use of sufficiently long and thin thermocouple wires on both sides of the junction. According to Bradley and co-authors [44] the conduction heat loss is assumed to be negligible if $l > 200 d_w$, where l is the length of the fine wire. However, a more detailed analysis by Petit and co-authors [45] reveals that a better criterion is to use wires of length l such that $l/l_c > 10$, in which l_c is the characteristic length defined as,

$$l_c = \sqrt{\frac{k_w d_w}{4 h_{conv}}}. \tag{22}$$

This criterion accounts for both the characteristics of the flow and of the sensor. Values obtained from applying Petit criterion to the thermocouples used in this study with the exposed wire of 10 mm length and wire diameter of 50 μm at different locations in and out of the flame, were found to be in the range of 14-17 for the l/l_c ratio which is above the recommended value of 10. Overall, the conduction error is considered negligible in this study.

Acknowledgments

The authors would like to acknowledge financial support for this work from the Minta Martin Foundation at the University of Maryland, College park.

References

[1] H. Emmons, ZAMM-Journal of Applied Mathematics and Mechanics/Zeitschrift für Angewandte Mathematik und Mechanik **36**, 60 (1956).

[2] F. J. Kosdon, F. A. Williams, and C. Buman, Proceedings of the Combustion Institute **12**, 253 (1969).

[3] J. Kim, J. de Ris, and F. Kroesser, Proceedings of the Combustion Institute **13**, 949 (1971).

[4] T. Hirano, K. Iwai, and Y. Kanno, Astronautica Acta **17**, 811 (1972).

[5] T. Hirano and Y. Kanno, Proceedings of the Combustion Institute **14**, 391 (1973).

[6] P. Pagni and T. Shih, Proceedings of the Combustion Institute **16**, 1329 (1977).

[7] T. Ahmad and G. M. Faeth, Proceedings of the Combustion Institute **17**, 1149 (1978).

[8] K. Annamalai and M. Sibulkin, Combustion Science and Technology **19**, 167 (1979).

[9] P. Andreussi and L. Petarca, Proceedings of the Combustion Institute **18**, 1861 (1981).

[10] A. V. Singh and M. J. Gollner, Proceedings of the Combustion Institute **35**, 2527 (2015).

[11] A. V. Singh and M. J. Gollner, Combustion and Flame **162**, 2214 (2015).

[12] T. H. Chilton and A. P. Colburn, Industrial & Engineering Chemistry **26**, 1183 (1934).

[13] R. Silver, Nature **165**, 725 (1950).

[14] D. Spalding, Fuel **29**, 2 (1950).

[15] S. Burke and T. Schumann, Proceedings of the Combustion Institute **1**, 2 (1948).

[16] D. B. Spalding, Proceedings of the Combustion Institute **4**, 847 (1953).

[17] P. J. Pagni, Fire Safety Journal **3**, 273 (1981).

[18] J. L. Torero, T. Vietoris, G. Legros, and P. Joulain, Combustion Science and Technology **174**, 187 (2002).

[19] W. Sirignano, Acta Astronautica **1**, 1285 (1974).

[20] F. A. Williams, *Proceedings of the Combustion Institute*, **16**, 1281 (1977).

[21] T. Hirano and M. Kinoshita, Proceedings of the Combustion Institute **15**, 379 (1975).

[22] P. Andreussi, Combustion and Flame **45**, 1 (1982).

[23] S. Andreotti, P. Andreussi, and L. Petarca, Combustion Science and Technology **40**, 279 (1984).

[24] J. S. Ha, S. H. Shim, and H. D. Shin, Combustion Science and Technology **75**, 241 (1991).

[25] D. Collis and M. Williams, Journal of Fluid Mechanics **6**, 357 (1959).

[26] M. du Plessis, R. Wang, and R. Kahawita, Journal of Fluids Engineering **96**, 246 (1974).

[27] A. Sfeir, International Journal of Heat and Mass Transfer **19**, 1289 (1976).

[28] P. Sforza, M. Steiger, and N. Trentacoste, AIAA journal **4**, 800 (1966).

[29] L. M. Jakob, *Heat Transfer: Vol. 1* (Wiley, 1967).

[30] G. Gubareff, J. Janssen, and R. Torborg, Minneapolis-Honeywell Regulator Company, Honeywell Research Center, Minneapolis (1960).

[31] V. Raghavan, A. Rangwala, and J. Torero, Combustion Theory and Modelling **13**, 121 (2009).

[32] F. P. Incropera, *Fundamentals of heat and mass transfer* (John Wiley & Sons, 2011).

[33] J. G. Quintiere, *Fundamentals of fire phenomena* (John Wiley and Sons, 2006).

[34] S. Turns, *An introduction to combustion*, Vol. 287 (McGraw-Hill, 1996).

[35] I. Glassman, *Combustion* (Academic press, 1997).

[36] F. Lockwood and A. Odidi, *Proceedings of the Combustion Institute*, **15**, 561 (1975).

[37] A. Ballantyne and J. Moss, Combustion Science and Technology **17**, 63 (1977).

[38] P. Miles and F. Gouldin, Combustion Science and Technology **89**, 181 (1993).

[39] A. Yule, D. Taylor, and N. Chigier, Journal of Energy **2**, 223 (1978).

[40] A. V. Singh, M. Yu, A. K. Gupta, and K. M. Bryden, Applied Energy **106**, 1 (2013).

[41] A. V. Singh, A. Eshaghi, M. Yu, A. K. Gupta, and K. M. Bryden, Applied Energy **115**, 116 (2014).

[42] C. R. Shaddix, in *33 rd National Heat Transfer Conference, Albuquerque, NM* (1999).

[43] C. D. Hodgman, R. C. Weast, and S. M. Selby, *Handbook of chemistry and physics: a ready-reference book of chemical and physical data* (Chemical Rubber Publishing Company, 1961).

[44] D. Bradley and K. Matthews, Journal of Mechanical Engineering Science **10**, 299 (1968).

[45] C. Petit, P. Gajan, J.-C. Lecordier, and P. Paranthoen, Journal of Physics E: Scientific Instruments **15**, 760 (1982).